ISSN 1674-1056
http://cpb.iphy.ac.cn
http://iopscience.iop.org/cpb
中国物理 B
Chinese Physics
中国物理 Chinese Physics B

Nonequilibrium free energy and information flow of a double quantum-dot system with Coulomb coupling

Zhiyuan Lin(林智远), Tong Fu(付彤), Juying Xiao(肖菊英), Shanhe Su(苏山河), Jincan Chen(陈金灿), and Yanchao Zhang(张艳超)

Citation: Chin. Phys. B, 2021, 30 (**8**): 080501. DOI: 10.1088/1674-1056/abe119
Journal homepage: http://cpb.iphy.ac.cn; http://iopscience.iop.org/cpb

What follows is a list of articles you may be interested in

Acoustic wireless communication based on parameter modulation and complex Lorenz chaotic systems with complex parameters and parametric attractors

Fang-Fang Zhang(张芳芳), Rui Gao(高瑞), and Jian Liu(刘坚)
Chin. Phys. B, 2021, 30 (**8**): 080503. DOI: 10.1088/1674-1056/ac0905

Nonequilibrium free energy and information flow of a double quantum-dot system with Coulomb coupling

Zhiyuan Lin(林智远), Tong Fu(付彤), Juying Xiao(肖菊英), Shanhe Su(苏山河)†, Jincan Chen(陈金灿), and Yanchao Zhang(张艳超)‡
Chin. Phys. B, 2021, 30 (**8**): 080501. DOI: 10.1088/1674-1056/abe119

Numerical investigation on photonic microwave generation by a sole excited-state emitting quantum dot laser with optical injection and optical feedback

Zai-Fu Jiang(蒋再富), Zheng-Mao Wu(吴正茂), Wen-Yan Yang(杨文艳), Chun-Xia Hu(胡春霞), Yan-Hong Jin(靳艳红), Zhen-Zhen Xiao(肖珍珍), and Guang-Qiong Xia(夏光琼)
Chin. Phys. B, 2021, 30 (**5**): 050504. DOI: 10.1088/1674-1056/abd2a8

Nonequilibrium thermodynamics and fluctuation relations for small systems

Cao Liang, Ke Pu, Qiao Li-Yan, Zheng Zhi-Gang
Chin. Phys. B, 2014, 23 (**7**): 070501. DOI: 10.1088/1674-1056/23/7/070501

Effects of anisotropy and magnetic fields on the specific heat of a quasi-two-dimensional Boltzmann gas in an elliptical parabolic quantum dot

Zhai Zhi-Yuan, Li Yu-Qi, Pan Xiao-Yin
Chin. Phys. B, 2012, 21 (**7**): 070506. DOI: 10.1088/1674-1056/21/7/070506

Nonequilibrium free energy and information flow of a double quantum-dot system with Coulomb coupling*

Zhiyuan Lin(林智远), Tong Fu(付彤), Juying Xiao(肖菊英), Shanhe Su(苏山河)†, Jincan Chen(陈金灿), and Yanchao Zhang(张艳超)‡

[1] *Department of Physics, Xiamen University, Xiamen* 361005, *China*
[2] *School of Science, Guangxi University of Science and Technology, Liuzhou* 545006, *China*

(Received 30 December 2020; revised manuscript received 20 January 2021; accepted manuscript online 29 January 2021)

We build a double quantum-dot system with Coulomb coupling and aim at studying connections among the entropy production, free energy, and information flow. By utilizing concepts in stochastic thermodynamics and graph theory analysis, Clausius and nonequilibrium free energy inequalities are built to interpret local second law of thermodynamics for subsystems. A fundamental set of cycle fluxes and affinities is identified to decompose two inequalities by using Schnakenberg's network theory. Results show that the thermodynamic irreversibility has energy-related and information-related contributions. A global cycle associated with the feedback-induced information flow would pump electrons against the bias voltage, which implements a Maxwell demon.

Keywords: quantum dot, nonequilibrium free energy, information, graph theory analysis

PACS: 05.70.Ln, 05.70.–a, 05.60.Gg, 05.90.+m **DOI:** 10.1088/1674-1056/abe119

1. Introduction

Irreversible thermodynamics is an extension of thermodynamics that studies transport phenomena such as the exchanges of mass, energy, and charge.[1] The Onsager reciprocity theorem expresses the rate of entropy production as the sum of the products of each flux and its conjugate affinity.[2–4] This thermodynamic relation is applicable for most far-from-equilibrium systems, even without accounting for the linear response regime. A nonzero affinity implies that a system is not in equilibrium and irreversible processes drive the system towards the state of equilibrium. The criterion for the selection of basic thermodynamic flows and forces remains a question worth exploring. For instance, the rate of entropy production of a thermoelectric device can be equivalently expressed in energy and heat representations.[5] Instead of collecting flows according to thermodynamic forces acting in the energy transduction, biogeochemical systems adopt basic graph concepts used in network analysis.[6]

Graph theory analysis indicates that some fundamental cycles make positive contribution to the total rate of entropy production in the ensemble.[7] Therefore, the cycles in graph may tell us the essential driving forces from the complex networks in living systems. Schnakenberg expressed the macroscopic entropy production of stochastic processes in terms of cycles from the network, because the products of the transition rates along a cycle depend only on the macroscopic thermodynamic affinities maintaining the system out of equilibrium.[8] Horowitz *et al.* used a graph theoretic method to provide a unified thermodynamic scheme describing information transfers in autonomous systems.[9] Yamamoto introduced a graph contraction method to prove that the Onsager coefficient associated with the driving of an information current satisfies the Onsager reciprocity.[10] Graph theory concepts have achieved great success at learning irreversible thermodynamics of the energy,[11,12] entropy, fluctuation,[13] and information at nanoscale.[14,15] Peusner developed network thermodynamics by combining theories of nonequilibrium thermodynamics, circuit theory, and graph theory to broaden applicability to biological systems.[16–22] The application of graph theory and network thermodynamics to analyze cycle fluxes, edge fluxes and energy transport processes in quantum systems may guide to design thermal nanodevices.

On the one hand, many studies were concerned with the formalism of free energy for irreversible thermodynamics. Crooks related nonequilibrium measurements of free energy differences to the work were performed on microscopically reversible Markovian systems.[23,24] The Jarzynski relation, which relates the free energy differences between two states to the irreversible work along an ensemble of trajectories joining the same states, has been often used for calculating the equilibrium free energies of classical and quantum systems.[25–28] Esposito introduced the concept of nonequilibrium system free energy to understand the irreversible work

*Project supported by the National Natural Science Foundation (Grant No. 11805159), the First Batch of National First-class Undergraduate Courses of China (2020), the Natural Science Foundation of Fujian Province, China (Grant No. 2019J05003), and Teaching Research Program of Thermodynamics and Statistical Physics in the Institution of Higher Education of China (2019).

†Corresponding author. E-mail: sushanhe@xmu.edu.cn
‡Corresponding author. E-mail: zhangyanchao@gxust.edu.cn

© 2021 Chinese Physical Society and IOP Publishing Ltd

in Hamiltonian dynamics of an open driven system.[29,30] More recently, the investigations of free energy were generalized to systems coupled to the environment with multiple heat baths.[31–34] Nonequilibrium Clausius and free energy inequalities are used to clarify the information and energy regimes in nonequilibrium systems.[35–43] Miyahara *et al.* derived the Sagawa–Ueda–Jarzynski relation under a non-isothermal system to measure the change of free energy.[34] Ptaszyński *et al.* formulated a nonequilibrium free energy inequality for a generic open quantum system weakly coupled to multi heat sources.[31] Despite recent developments, relatively little attention has been paid to correlate the non-equilibrium free energy in terms of thermodynamic affinities and flows. By considering the great success of graph theory analysis in irreversible thermodynamics, a cycle decomposition may help to establish this connection.

Considering a double-quantum-dot system, we will employ graph theory to analyze the entropy production and the non-equilibrium free energy of an open quantum system obeying continuous-time Markov jump process. The contents are organized as follows: In Section 2, the general model of two quantum dots coupled in parallel to four electronic reservoirs with different chemical potentials is briefly described. Schnakenberg's network theory is applied to obtain fundamental cycle fluxes and affinities. Nonequilibrium Clausius and free energy inequalities of subsystems at steady state are derived. In Section 3, thermodynamic characteristic functions varying with the Coulomb coupling strength will be evaluated numerically. Finally, main conclusions are drawn.

2. Model and methods

2.1. The double quantum-dot system with Coulomb coupling

The considered model is a bipartite system that consists of capacitively coupled quantum dots X and Y, as shown in Fig. 1(a). The quantum dots X and Y with energies ε_X and ε_Y are coupled via the long-range Coulomb force U such that they only exchange energy but no electrons. The states of the composite system are given by a four-state basis $z = \{|(x_0,y_0)\rangle, |(x_1,y_0)\rangle, |(x_0,y_1)\rangle, |(x_1,y_1)\rangle\}$, where x_0 and y_0 (x_1 and y_1) represent that the site of X and Y is empty (filled), respectively. The quantum dot X (Y) is connected to two Fermi reservoirs XL and XR (YL and YR) and admits electron transports through parallel interacting channels. Figure 1(b) is the equivalent circuit showing the capacitive couplings between quantum dots and reservoirs. $V_\nu = \mu_\nu/e$ ($\nu = XL, XR, YL, YR$) determines the voltage of reservoir ν, where μ_ν is the chemical potential and e is the elementary positive charge. The imbalance capacitances between the quantum dot and the terminal ν and between X and Y are defined as C_ν and C, respectively; ϕ_x and ϕ_y are the electrostatic potentials in each quantum dot at state $|(x,y)\rangle$. The total charges of X and Y at state $|(x,y)\rangle$ are the sum of charges on all of capacitors connected to X and Y,[44,45] i.e.,

$$\begin{aligned} q_x &= C_{XL}(\phi_x - V_{XL}) + C_{XR}(\phi_x - V_{XR}) \\ &\quad + C(\phi_x - \phi_y), \end{aligned} \tag{1}$$

$$\begin{aligned} q_y &= C_{YL}(\phi_y - V_{YL}) + C_{YR}(\phi_y - V_{YR}) \\ &\quad + C(\phi_y - \phi_x). \end{aligned} \tag{2}$$

These two equations can be expressed more compactly in a matrix form

$$\begin{bmatrix} q_x + C_{XL}V_{XL} + C_{XR}V_{XR} \\ q_y + C_{YL}V_{YL} + C_{YR}V_{YR} \end{bmatrix} = \begin{bmatrix} C'_X & -C \\ -C & C'_Y \end{bmatrix} \begin{bmatrix} \phi_x \\ \phi_y \end{bmatrix}, \tag{3}$$

where $C'_X = C_{XL} + C_{XR} + C$ and $C'_Y = C_{YL} + C_{YR} + C$ define the total capacitances of X and Y. The electrostatic potentials ϕ_x and ϕ_y are then conveniently expressed using the capacitance matrix

$$\begin{aligned} \begin{bmatrix} \phi_x \\ \phi_y \end{bmatrix} &= \frac{1}{C'_X C'_Y - C^2} \begin{bmatrix} C'_Y & C \\ C & C'_X \end{bmatrix} \\ &\quad \times \begin{bmatrix} q_x + C_{XL}V_{XL} + C_{XR}V_{XR} \\ q_y + C_{YL}V_{YL} + C_{YR}V_{YR} \end{bmatrix}. \end{aligned} \tag{4}$$

The electrostatic energy for a given quantum state is computed by

$$\begin{aligned} U(x,y) &= \frac{1}{2}\left[q_x + C_{XL}V_{XL} + C_{XR}V_{XR}, q_y \right. \\ &\quad \left. + C_{YL}V_{YL} + C_{YR}V_{YR}\right] \begin{bmatrix} \phi_x \\ \phi_y \end{bmatrix}. \end{aligned} \tag{5}$$

Note that $q_x(q_y) = 0$ or e, depending on whether $X(Y)$ is empty or occupied. Thus, the electrostatic energies for the four quantum states read

$$\begin{aligned} U(x_0,y_0) &= \frac{1}{2(C'_X C'_Y - C^2)} \\ &\quad \times \left(C'_Y \mathcal{Q}_x^2 + 2C\mathcal{Q}_x\mathcal{Q}_y + C'_X \mathcal{Q}_y^2\right), \\ U(x_1,y_0) &= \frac{1}{2(C'_X C'_Y - C^2)} \\ &\quad \times \left[C'_Y\left(e^2 + 2e\mathcal{Q}_x\right) + 2eC\mathcal{Q}_y\right] + U_{x_0y_0}, \\ U(x_0,y_1) &= \frac{1}{2(C'_X C'_Y - C^2)} \\ &\quad \times \left[2eC\mathcal{Q}_x + C'_X\left(e^2 + 2e\mathcal{Q}_y\right)\right] + U_{x_0y_0}, \\ U(x_1,y_1) &= \frac{2e^2C}{2(C'_X C'_Y - C^2)} \\ &\quad + U_{x_1y_0} + U_{x_0y_1} - U_{x_0y_0}, \end{aligned} \tag{6}$$

where $\mathcal{Q}_x = C_{XL}V_{XL} + C_{XR}V_{XR}$ and $\mathcal{Q}_y = C_{YL}V_{YL} + C_{YR}V_{YR}$. We are now capable of determining the change of energy in the system when an electron tunnels into a quantum dot. When the other dot is empty, the charging energies of X and Y are, respectively, given by

$$U_{X_0} = U(x_1,y_0) - U(x_0,y_0),$$

$$U_{Y_0} = U(x_0, y_1) - U(x_0, y_0). \tag{7}$$

On the other hand, when the other dot is occupied, the charging energies of X and Y are, respectively, expressed as

$$\begin{aligned} U_{X_1} &= U(x_1, y_1) - U(x_0, y_1), \\ U_{Y_1} &= U(x_1, y_1) - U(x_1, y_0). \end{aligned} \tag{8}$$

The differences of charging energies $U_{X_1} - U_{X_0} = U_{Y_1} - U_{Y_0} = U$, where $U = q^2 C / \left(C'_X C'_Y - C^2\right)$ determines the quantized energy which can be transferred from one dot to the other.

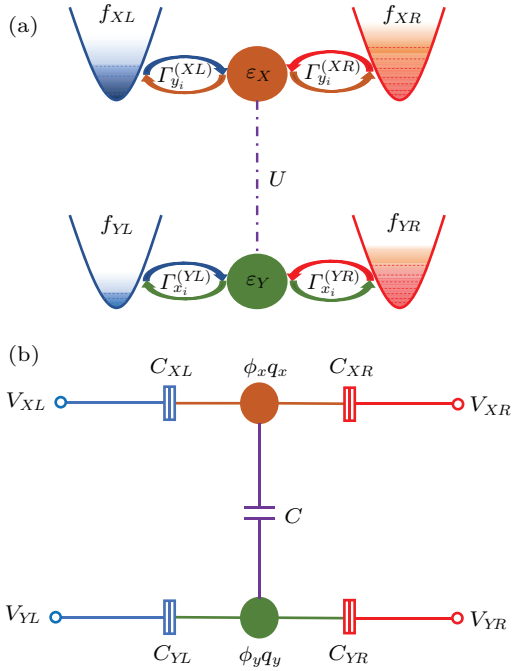


Fig. 1. The schematic diagram of a Coulomb-coupled double quantum-dot system. (b) The equivalent circuit showing the capacitive couplings between quantum dots and reservoirs. Each dot connects to an electron reservoir ν via the tunneling junction with junction resistance R_ν and capacitance C_ν in parallel.

2.2. The master equation

Let $p(z,t)$ be the probability of state z of the coupled quantum dots at time t. In the regime of sequential tunneling approximation, the broadening of energy levels can be neglected and the transmission through tunnel barriers is defined by the sequential tunneling of a single electron. Thus, the time evolution of $p(z,t)$ is governed by a Markovian master equation[46–48]

$$\frac{\mathrm{d}}{\mathrm{d}t} p(z,t) = \sum_{z',\nu} \left[R_{zz'}^{(\nu)} p(z',t) - R_{z'z}^{(\nu)} p(z,t) \right]. \tag{9}$$

The transition rate from state z' to state z induced by reservoir ν reads

$$R_{zz'}^{(\nu)} = \begin{cases} R_{xx'|y}^{(\nu)} & (x \neq x', y = y', \nu = XL, XR), \\ R_{yy'|x}^{(\nu)} & (x = x', y \neq y', \nu = YL, YR), \\ 0 & (\text{otherwise}), \end{cases} \tag{10}$$

where $x' \in \{x_0, x_1\}$ and $y' \in \{y_0, y_1\}$. We have assumed that the two subsystems should not change their states simultaneously during a single transition process. The transition rates follow from Fermi's golden rule[49–51] and are given by

$$\begin{aligned} R_{x_1 x_0|y_i}^{(\nu)} &= \Gamma_{y_i}^{(\nu)} f_{y_i}^{(\nu)}, \\ R_{x_0 x_1|y_i}^{(\nu)} &= \Gamma_{y_i}^{(\nu)} \left(1 - f_{y_i}^{(\nu)}\right), \\ R_{y_1 y_0|x_i}^{(\nu)} &= \Gamma_{x_i}^{(\nu)} f_{x_i}^{(\nu)}, \\ R_{y_0 y_1|x_i}^{(\nu)} &= \Gamma_{x_i}^{(\nu)} \left(1 - f_{x_i}^{(\nu)}\right), \end{aligned} \tag{11}$$

where $R_{x_1 x_0|y_i}^{(\nu)}$ and $R_{x_0 x_1|y_i}^{(\nu)}$ describe electron transfers in and out of dot X through reservoir ν, respectively. $R_{y_1 y_0|x_i}^{(\nu)}$ and $R_{y_0 y_1|x_i}^{(\nu)}$ are the transfer rates of electron in and out of dot Y. Here $f_{x_i}^{(\nu)} = \left\{1 + \exp\left[\beta_\nu \left(\varepsilon_Y + U_{Y_0} + \mathrm{i}U - \mu_\nu\right)\right]\right\}^{-1}$ and $f_{y_i}^{(\nu)} = \left\{1 + \exp\left[\beta_\nu \left(\varepsilon_X + U_{X_0} + \mathrm{i}U - \mu_\nu\right)\right]\right\}^{-1}$ $(i = 0, 1)$ are the Fermi-Dirac distribution functions of reservoir ν at temperature T_ν and chemical potential μ_ν. All temperatures are set to be equal, i.e., $T_\nu = T$. The inverse temperature parameter $\beta_\nu = 1/(k_\mathrm{B} T_\nu)$, where k_B is Boltzmann's constant and we set $k_\mathrm{B} = 1$ in the discussion. $\Gamma_{x_i}^{(\nu)}$ $(\Gamma_{y_i}^{(\nu)})$ is a positive constant describing the height of the potential barrier between dot Y (X) and reservoir ν. The potential barrier of Y, characterized by $\Gamma_{x_i}^{(\nu)}$, depends on the state of X, and vice versa.

2.3. Schnakenberg's network theory

Schnakenberg stated that nonequilibrium random processes could be investigated and understood by carrying out the graph analysis associated with the master equation.[8,10,13] For purposes of relating thermodynamic properties to fundamental fluxes and affinities, a graph representation of the dynamics of the double quantum-dot system is introduced. Instead of using the master equations, the graph representation in Fig. 2 identifies a fundamental set of cycles of the quantum network. We will show that it is the fluxes associated with the cycle basis that captures the mesoscopic currents for energy and information transfers, which allows us to understand the irreversible thermodynamics in a more intuitive way. Nevertheless, one should note that because Schnakenberg developed the network theory using the method of Kirchhoff's circuit laws to determine the steady state solution,[13] the exact time evolution of a nonequilibrium small system can only be solved by the master equation.

According to Schnakenberg's network theory, a vertex in the graph G represents a state of the system z. As shown in Fig. 2, the dark-orange circle represents the state of dot X, while the dark-green circle shows the state of dot Y. They are either completely filled or completely empty, indicating that the corresponding quantum dot is filled with one electron or not. A red double-headed arrow stands for forward and backward transitions between two states $(x,y) \Longleftrightarrow (x',y')$. Two

arbitrary states can be connected by several edges if several elementary processes allow transitions between them. A directed edge $e := \left(z' \xrightarrow{\nu} z\right)$ (the single-headed curly arrow of a cycle with a directed orientation) is corresponding to the transition from state z' to state z through reservoir ν with a nonzero transition rate $R^{(\nu)}_{zz'}$. One can arbitrarily choose the direction of an edge, such as the directed graph in Fig. 2. For edge e, the edge affinity and edge current are, respectively, defined by

$$\mathcal{F}_{\rm e} = \ln \frac{R^{(\nu)}_{zz'}}{R^{(\nu)}_{z'z}}, \tag{12}$$

$$J_{\rm e} = R^{(\nu)}_{zz'} p(z',t) - R^{(\nu)}_{z'z} p(z,t). \tag{13}$$

We next define the effective affinity of edge e as

$$\mathcal{F}_{\rm e} := \mathcal{F}_{\rm e} + \ln \frac{p(z',t)}{p(z,t)}. \tag{14}$$

Because $J_{\rm e} = 0$ results in $\mathcal{F}_{\rm e} = 0$, the effective affinity acts as the conjugate of current $J_{\rm e}$. In contrast, $\mathcal{F}_{\rm e}$ can be regarded as the bare thermodynamic affinity related to the detailed balance.

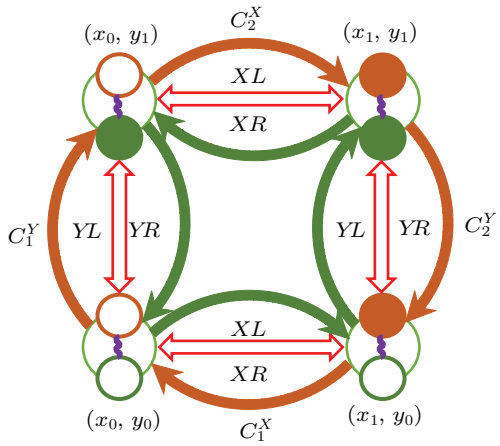


Fig. 2. Illustration of the directed graph G and the cycle basis. The vertices represent the four states of the two quantum dots, and a double-headed arrow stands for forward and backward transitions between two states induced by a reservoir. The single-headed curly arrows are the edges of a cycle basis with a directed orientation. Note that we can arbitrarily choose the direction of an edge.

According to Kirchhoff's current law,[8] the stationary Master equation [Eq. (9) with $\frac{\rm d}{{\rm d}t} p(z,t) = 0$] leads to

$$\sum_{z',\nu} J_{\rm e} = 0. \tag{15}$$

By specifying the set $\mathcal{E}$ as a collection of directed edges (represented by the single-headed curly arrows) in Fig. 2, we have $(z' \to z) \in \mathcal{E} \Rightarrow (z \to z') \notin \mathcal{E}$. Under the assignment in Eq. (10), each edge only describes a transition in X or Y. Therefore, one can use the set $\mathcal{E}^X := \left\{e = \left((x',y) \xrightarrow{\nu} (x,y)\right) \in \mathcal{E}\right\} (x \neq x')$ to describe transitions in X and the other set $\mathcal{E}^Y := \left\{e = \left((x,y') \xrightarrow{\nu} (x,y)\right) \in \mathcal{E}\right\} (y \neq y')$ to cover transitions in Y. The set $\mathcal{E}$ of all edges is then divided into two parts $\mathcal{E}^X$ and $\mathcal{E}^Y$.

The method to identify the fundamental cycles of the graph is based on the definition of a maximal tree $T(G)$ of the graph G, which satisfies the following properties: Firstly, a maximal tree $T(G)$ is a subgraph of Fig. 2, which contains all the vertices. All the edges of $T(G)$ are edges of Fig. 2 and are connected. Secondly, the maximal tree $T(G)$ contains no cycle, i.e., no cyclic sequence of edges. Obviously, the four state model has four type of maximal tree. We choose one of the maximal tree $T(G)$, as shown in Fig. 3(a). The edges, which are the edges of the graph but do not belong to the edges in Fig. 3(a), are called the chords of the maximal tree. If we add a chord l ($l \in \mathcal{E}$ and $l \notin T(G)$) to the maximal tree $T(G)$, the resulting subgraph contains exactly one basis cycle by removing all the edges which are not part of the circuit from $T(G) + l$. By following the above description and assigning an arbitrary orientation, the set of fundamental circuits $\mathcal{C}_0 = \{C_1, C_2, C_3, C_4, C_5\}$ can be obtained, as shown in Fig. 3(b). A maximal tree together with its associated fundamental set of cycles $\mathcal{C}_0$ provides a decomposition of the graph G. It can be chosen arbitrarily because each cycle in $\mathcal{C}_0$ can be redefined by linear combinations of the cycles of the fundamental set. We next introduce a directed cycle as a directed sequence of connected edges with the same initial and terminal vertex. According to the assignments of the directions of edges in Fig. 2, the circuit C_5 cannot form a directed cycle. The circuits C_4 and C_5 are linearly combined to define circuit C_6. Figure 3(c) shows that C_6 contains all edges of C_4 and C_5, which do not simultaneously belong to C_4 and C_5.

Assigning orientations to the circuits C_1, C_2, C_3, C_4, and C_6, one can now define a cycle basis of the directed graph (Fig. 2) $\mathcal{C} = \{C_1^X, C_2^X, C_1^G, C_1^Y, C_2^Y\}$ as

$$\begin{aligned}
C_1^X &:= \left\{(x_0,y_0) \xrightarrow{XL} (x_1,y_0) \xrightarrow{XR} (x_0,y_0)\right\},\\
C_2^X &:= \left\{(x_0,y_1) \xrightarrow{XL} (x_1,y_1) \xrightarrow{XR} (x_0,y_1)\right\},\\
C_1^Y &:= \left\{(x_0,y_0) \xrightarrow{YL} (x_0,y_1) \xrightarrow{YR} (x_0,y_0)\right\},\\
C_2^Y &:= \left\{(x_1,y_0) \xrightarrow{YL} (x_1,y_1) \xrightarrow{YR} (x_1,y_0)\right\},\\
C_1^G &:= \left\{(x_0,y_0) \xrightarrow{YL} (x_0,y_1) \xrightarrow{XL} (x_1,y_1)\right.\\
&\quad \left. \xrightarrow{YL} (x_1,y_0) \xrightarrow{XL} (x_0,y_0)\right\}.
\end{aligned} \tag{16}$$

This set of cycles is broadly classified into three groups: local cycles of X, $\mathcal{C}^X := \{C_1^X, C_2^X\}$; local cycles of Y, $\mathcal{C}^Y := \{C_1^Y, C_2^Y\}$; and a global cycle, $\mathcal{C}^G := C_1^G$. A local cycle indicates that $X(Y)$ is fixed and $Y(X)$ is changing, which supports internal subsystem flows. The global cycle C_1^G links X and Y, so that a current flowing around a global cycle carries energy and entropy from one subsystem to the other. Any other cycles

are recognized as a linear combination of cycles in $\mathcal{C}$.[9] It will be useful to introduce the function

$$\Xi\left(e,C_k\right):=\begin{cases}1 & \left(e\in C_k^l\right),\\ -1 & \left(e^{\dagger}\in C_k^l\right),\\ 0 & (\text{otherwise}),\end{cases} \tag{17}$$

where $e\in C_k^l\,(l=X,Y,G;k=1,2)$ means that e is one of edges in C_k^l, and $e^{\dagger}:=\left(z\xrightarrow{\nu}z'\right)$ defines the backward transition edge of e. To each fundamental cycle, one can then assign the affinity $\mathcal{F}\left(C_k^l\right)$ as a sum of affinities along edges in C_k^l,

$$\mathcal{F}\left(C_k^l\right):=\sum_{\mathrm{e}\in\mathcal{E}}\Xi\left(e,C_k^l\right)\mathcal{F}_{\mathrm{e}}. \tag{18}$$

The motive is to introduce partial affinities of cycles associated with X and Y by

$$\mathcal{F}_X\left(C_k^l\right)=\sum_{\mathrm{e}\in\mathcal{E}^{\mathrm{X}}}\Xi\left(e,C_k^l\right)F_{\mathrm{e}}, \tag{19}$$

$$\mathcal{F}_Y\left(C_k^l\right)=\sum_{\mathrm{e}\in\mathcal{E}^{\mathrm{Y}}}\Xi\left(e,C_k^l\right)F_{\mathrm{e}}. \tag{20}$$

Note that partial affinities are found to be dissimilar to $\mathcal{F}\left(C_k^l\right)$, because the sums are not taken over $\mathcal{E}$ but over $\mathcal{E}^X$ and $\mathcal{E}^Y$.

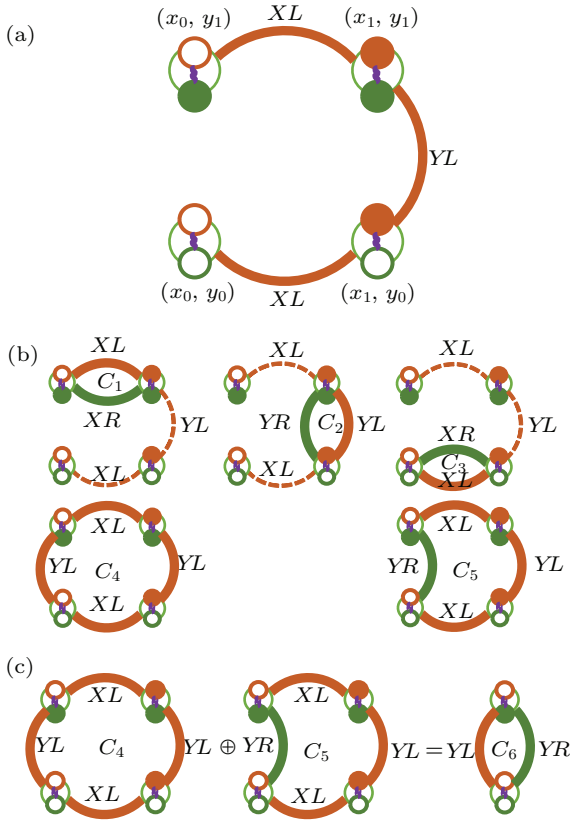


Fig. 3. (a) A maximal tree $T(G)$ of the graph G. (b) The fundamental set of circuits $\mathcal{C}=\{C_1^X,C_2^X,C_1^G,C_2^G,C_1^Y\}$ for the maximal tree $T(G)$. (c) The linear combination relation $C_4\oplus C_5=C_6$.

Using the definition in Eq. (14), one can also define the effective affinity of C_k^l as

$$\mathscr{F}\left(C_k^l\right):=\sum_{\mathrm{e}\in\mathcal{E}}\Xi\left(e,C_k^l\right)\mathcal{F}_{\mathrm{e}}. \tag{21}$$

Partial effective affinities of cycles corresponding to X and Y are written as

$$\mathscr{F}_X\left(C_k^l\right)=\sum_{\mathrm{e}\in\mathcal{E}^{\mathrm{X}}}\Xi\left(e,C_k^l\right)\mathcal{F}_{\mathrm{e}}, \tag{22}$$

$$\mathscr{F}_Y\left(C_k^l\right)=\sum_{\mathrm{e}\in\mathcal{E}^{\mathrm{Y}}}\Xi\left(e,C_k^l\right)\mathcal{F}_{\mathrm{e}}. \tag{23}$$

Combining Eqs. (21)–(23) with Eqs. (12) and (17), one can obtain effective affinities of local cycles and partial effective affinities of the global cycle in Eq. (16),

$$\mathscr{F}(C_1^X)=\mathscr{F}(C_2^X):=-\Delta\mu_X/T, \tag{24}$$

$$\mathscr{F}(C_1^Y)=\mathscr{F}(C_2^Y):=-\Delta\mu_Y/T, \tag{25}$$

$$\mathscr{F}_X\left(C_1^G\right)=-\mathscr{F}_Y\left(C_1^G\right)=\ln\frac{p\left(x_0,y_1\right)p\left(x_1,y_0\right)}{p\left(x_0,y_0\right)p\left(x_1,y_1\right)}-U/T, \tag{26}$$

where $\Delta\mu_X=\mu_{XR}-\mu_{XL}$ and $\Delta\mu_Y=\mu_{YR}-\mu_{YL}$. For the global cycle C_1^G, the partial affinities $\mathcal{F}_X\left(C_1^G\right)=-\mathcal{F}_Y\left(C_1^G\right)=-U/T$. The partial effective affinities of the global cycle in Eq. (26) is equal to the sum of the two forces, i.e.,

$$\mathscr{F}_X\left(C_1^G\right)=\mathcal{F}_X\left(C_1^G\right)+\mathcal{F}_I\left(C_1^G\right), \tag{27}$$

$$\mathscr{F}_Y\left(C_1^G\right)=\mathcal{F}_Y\left(C_1^G\right)-\mathcal{F}_I\left(C_1^G\right), \tag{28}$$

where $\mathcal{F}_I\left(C_1^G\right)=\ln\frac{p(x_0,y_1)p(x_1,y_0)}{p(x_0,y_0)p(x_1,y_1)}$ provides the driving force for information exchanges between X and Y. The information affinity is only contained in the partial effective affinities of the global cycle.

Transitions around cycle C_k^l generate the net current $J\left(C_k^l\right)$ (cycle current), which is fundamental in irreversible thermodynamics. At steady state, Kirchhoff's laws govern the conservation of energy and charge, indicating that

$$J_{\mathrm{e}}=\sum_{C_k^l\in\mathcal{C}}\Xi\left(e,C_k^l\right)J\left(C_k^l\right). \tag{29}$$

Therefore, currents corresponding to basic cycles [Eq. (16)] can be calculated as

$$\begin{aligned}
J(C_1^X)&:=R^{(XR)}_{x_0x_1|y_0}p(x_1,y_0)-R^{(XR)}_{x_1x_0|y_0}p(x_0,y_0)=J^{(XR)}_{x_0x_1|y_0},\\
J(C_2^X)&:=R^{(XR)}_{x_0x_1|y_1}p(x_1,y_1)-R^{(XR)}_{x_1x_0|y_1}p(x_0,y_1)=J^{(XR)}_{x_0x_1|y_1},\\
J(C_1^G)&:=\left(R^{(YL)}_{y_1y_0|x_0}+R^{(YR)}_{y_1y_0|x_0}\right)p(x_0,y_0)\\
&\quad-\left(R^{(YL)}_{y_0y_1|x_0}+R^{(YR)}_{y_0y_1|x_0}\right)p(x_0,y_1)\\
&=J^{(YL)}_{y_1y_0|x_0}+J^{(YR)}_{y_1y_0|x_0},\\
J(C_1^Y)&:=R^{(YR)}_{y_0y_1|x_0}p(x_0,y_1)-R^{(YR)}_{y_1y_0|x_0}p(x_0,y_0)=J^{(YR)}_{y_0y_1|x_0},\\
J(C_2^Y)&:=R^{(YR)}_{y_0y_1|x_1}p(x_1,y_1)-R^{(YR)}_{y_1y_0|x_1}p(x_1,y_0)=J^{(YR)}_{y_0y_1|x_1},
\end{aligned} \tag{30}$$

where $J^{(\nu)}_{xx'|y}$ represents the current due to the transition $(x',y)\xrightarrow{\nu}(x,y)$, and similarly for $J^{(\nu)}_{yy'|x}$.

Net electronic currents from XR and XL and from YR and YL are, respectively, simplified to

$$J_X=-\left(J(C_1^X)+J(C_2^X)\right), \tag{31}$$

$$J_Y=-\left(J(C_1^Y)+J(C_2^Y)\right). \tag{32}$$

2.4. Nonequilibrium Clausius inequalities of the two subsystems

Given the probability of a microstate, the entropy of the system can be written as[25,52,53]

$$S(t) = -\sum_{z} p(z,t)\ln p(z,t). \tag{33}$$

For steady states, the time derivative of Eq. (33) reduces to

$$\dot{S} = \dot{\sigma} + \dot{S}_{\rm r} = 0, \tag{34}$$

where

$$\dot{\sigma} = \sum_{\nu}\sum_{z,z'} R^{(\nu)}_{zz'} p\left(z',t\right)\ln\frac{R^{(\nu)}_{zz'}p\left(z',t\right)}{R^{(\nu)}_{z'z}p(z,t)} \tag{35}$$

is the rate of total entropy production,[54] and

$$\dot{S}_r = -\sum_{\nu}\sum_{z,z'} R^{(\nu)}_{zz'} p\left(z',t\right)\ln\frac{R^{(\nu)}_{zz'}}{R^{(\nu)}_{z'z}} = -\sum_{\mathrm{e}\in\mathcal{E}} J_{\mathrm{e}}\mathcal{F}_{\mathrm{e}} \tag{36}$$

describes the entropy flow from reservoirs.

The Logarithmic sum inequality states that for nonnegative a_i and b_i, $\sum_{i=1}^{n} a_i \ln\frac{a_i}{b_i} \geq a\ln\frac{a}{b}$ with $a=\sum_i a_i$ and $b=\sum_i b_i$. Therefore, one can prove that $\dot{\sigma}\geq 0$ and the second law of thermodynamics holds for the system. Note that the second equality in Eq. (36) results from the definitions of edge affinities and edge currents in Eqs. (12) and (13). In the long time limit, the system reaches a unique non-equilibrium stationary state and $\dot{S}=0$. The rate of entropy production must be balanced by entropy flows through its terminals, i.e., $\dot{\sigma}=-\dot{S}_r$, which is the sum of the affinities multiplied by the currents as well.

Transition rates [Eq. (11)] between different states satisfy local detailed balances, e.g.,

$$\ln\frac{R^{(XR)}_{x_1x_0|y_0}}{R^{(XR)}_{x_0x_1|y_0}} = -\left(\varepsilon'_X-\mu_{XR}\right)/T,$$
$$\ln\frac{R^{(XR)}_{x_1x_0|y_1}}{R^{(XR)}_{x_0x_1|y_1}} = -\left(\varepsilon'_X+U-\mu_{XR}\right)/T.$$

Thus, the entropy flow is simplified to

$$\dot{S}_r = -\left(J_X\Delta\mu_X + J_Y\Delta\mu_Y\right)/T. \tag{37}$$

From the first law of thermodynamics, each electron leaving an electron reservoir removes energy equal to the difference between its total energy and the chemical potential of the reservoir.[55] Therefore, for the interaction between X and reservoir XR, $\varepsilon'_X-\mu_{XR}$ and $\varepsilon'_X+U-\mu_{XR}$ represent thermal energies supplied by reservoir XR during a jump in the subsystem X, which enables us to identify the heat current into X from reservoir XR

$$\dot{Q}_{XR} = T\left(J^{(XR)}_{x_0x_1|y_0}\ln\frac{R^{(XR)}_{x_1x_0|y_0}}{R^{(XR)}_{x_0x_1|y_0}} + J^{(XR)}_{x_0x_1|y_1}\ln\frac{R^{(XR)}_{x_1x_0|y_1}}{R^{(XR)}_{x_0x_1|y_1}}\right)$$
$$= -J^{(XR)}_{x_0x_1|y_0}\left(\varepsilon'_X-\mu_{XR}\right) - J^{(XR)}_{x_0x_1|y_1}\left(\varepsilon'_X+U-\mu_{XR}\right). \tag{38}$$

By following the same path, heat currents into the system from reservoirs XL, YR, and YL are, respectively, given by

$$\dot{Q}_{XL} = J^{(XL)}_{x_1x_0|y_0}\left(\varepsilon'_X-\mu_{XL}\right) + J^{(XL)}_{x_1x_0|y_1}\left(\varepsilon'_X+U-\mu_{XL}\right), \tag{39}$$
$$\dot{Q}_{YR} = -J^{(YR)}_{y_0y_1|x_0}\left(\varepsilon'_Y-\mu_{YR}\right) - J^{(YR)}_{y_0y_1|x_1}\left(\varepsilon'_Y+U-\mu_{YR}\right), \tag{40}$$
$$\dot{Q}_{YL} = J^{(YL)}_{y_1y_0|x_0}\left(\varepsilon'_Y-\mu_{YL}\right) + J^{(YL)}_{y_1y_0|x_1}\left(\varepsilon'_Y+U-\mu_{YL}\right). \tag{41}$$

The rate of total entropy production can be conveniently related to heat currents by summing up Eqs. (38)–(41), i.e.,

$$\dot{\sigma} = -\dot{S}_r = -\sum_{\nu}\dot{Q}_\nu/T \geq 0. \tag{42}$$

Equations (33)–(37) exclusively explain the entropy flow between the system and the environment. To clarify how energy and information are exchanged between the two subsystems, we introduce the rates of partial entropy production associated with X and Y as[9,56]

$$\dot{\sigma}_X = \sum_{\nu}\sum_{x\geq x',y} J^{(\nu)}_{xx'|y}\ln\frac{R^{(\nu)}_{xx'|y}p\left(x',y\right)}{R^{(\nu)}_{x'x|y}p(x,y)}, \tag{43}$$

$$\dot{\sigma}_Y = \sum_{\nu}\sum_{x,y\geq y'} J^{(\nu)}_{yy'|x}\ln\frac{R^{(\nu)}_{yy'|x}p\left(x,y'\right)}{R^{(\nu)}_{y'y|x}p(x,y)}. \tag{44}$$

In addition, the rate of total entropy production can then be divided into two separate parts followed by

$$\dot{\sigma} = \dot{\sigma}_X + \dot{\sigma}_Y. \tag{45}$$

These classification can be proved directly from the relation $\sum_{z'} J_{\mathrm{e}} = \sum_{\nu,x'} J^{(\nu)}_{xx'|y} + \sum_{\nu,y'} J^{(\nu)}_{yy'|x}$ and the prescribed transition rate [Eq. (10)]. The logarithmic sum inequality again shows that $\dot{\sigma}_X$ and $\dot{\sigma}_Y$ are nonnegative individually, i.e.,

$$\dot{\sigma}_X \geq 0, \quad \dot{\sigma}_Y \geq 0, \tag{46}$$

which is a generalized second law of thermodynamics stronger than Eq. (42). Not only the rate of total entropy production but also the rates of partial entropy production must be nonnegative for the bipartite system. The information exchange between X and Y enforces positive values of $\dot{\sigma}_X$ and $\dot{\sigma}_Y$. The reasons become clear when dividing Eqs. (43) and (44) into three components,

$$\dot{\sigma}_X = \dot{\sigma}_{\mu_X} + \dot{\sigma}_{U_X} - \dot{I}_X, \tag{47}$$
$$\dot{\sigma}_Y = \dot{\sigma}_{\mu_Y} + \dot{\sigma}_{U_Y} - \dot{I}_Y, \tag{48}$$

where

$$\dot{\sigma}_{\mu_X} = \mathcal{F}(C^X_1)\left(J\left(C^X_1\right) + J\left(C^X_2\right)\right),$$
$$\dot{\sigma}_{\mu_Y} = \mathcal{F}(C^Y_1)\left(J\left(C^Y_1\right) + J\left(C^Y_2\right)\right),$$

$$\begin{aligned}
\dot{\sigma}_{U_X} &= \mathcal{F}_X\left(C_1^G\right) J\left(C_1^G\right), \\
\dot{\sigma}_{U_Y} &= \mathcal{F}_Y\left(C_1^G\right) J\left(C_1^G\right), \\
\dot{I}_X &= -J\left(C_1^G\right) \mathcal{F}_I\left(C_1^G\right), \\
\dot{I}_Y &= J\left(C_1^G\right) \mathcal{F}_I\left(C_1^G\right).
\end{aligned} \tag{49}$$

The first term $\dot{\sigma}_{\mu_{X(Y)}}$ indicates that the local cycle $C_k^{X(Y)}$ having a local affinity $\mathcal{F}(C_k^{X(Y)})$ supports internal flows within the subsystem. The global cycle C_1^G generates a global current $J\left(C_1^G\right)$ to carry the energy and information from one subsystem to the other. $\dot{\sigma}_{U_X}$ and $\dot{\sigma}_{U_Y}$ are responsible for the direct energy transfer between X and Y due to the Coulomb coupling. Any energy extracted by the partial affinity $\mathcal{F}_X\left(C_1^G\right)$ will be deposited in Y's environment by $\mathcal{F}_Y\left(C_1^G\right)$. The information flow $\dot{I}_{X(Y)}$ exclusively occurs on the global cycle C_1^G with information affinity $\mp\mathcal{F}_I\left(C_1^G\right)$. When $\mathcal{F}_X\left(C_1^G\right) \ll \mathcal{F}_I\left(C_1^G\right)$, the dominant force is information for driving X. On the other hand, when $\mathcal{F}_X\left(C_1^G\right) \gg \mathcal{F}_I\left(C_1^G\right)$, the interaction is mainly powered by energy. The cycle graph analysis enables a better understanding of the driving mechanisms of internal interactions. It is worth pointing out that Ref. [8] provided an important and enlightening formalism describing the graph representation of the systemic dynamics and computed the contribution of the thermodynamic cycles to entropy balances and Clausius inequalities. The present work follows the pioneer theory of Ref. [8]. However, we are more interested in deriving inequalities characterizing nonequilibrium free energy balances for the subsystems of a composite system. By correlating thermodynamic functions in terms of the affinities and flows of fundamental cycles, we identify energy-related and information-related contributions to local nonequilibrium free energy rates.

2.5. Nonequilibrium free energy inequalities of the two subsystems

The work flux produced by each channel is equal to the net electronic current along X or Y multiplied by the bias voltage of the corresponding circuit. Since $\mathcal{F}(C_1^{X(Y)})$ takes the chemical potential difference as the thermodynamic driving force and $J(C_1^{X(Y)}) + J(C_2^{X(Y)})$ represents the net electronic current along $X(Y)$, the work flux $W_{X(Y)}$ performed on a subsystem is identified to

$$\begin{aligned}
\dot{W}_{X(Y)} &= T\mathcal{F}(C_1^{X(Y)}) \left[J\left(C_1^{X(Y)}\right) + J\left(C_2^{X(Y)}\right)\right] \\
&= -T\mathcal{F}(C_1^{X(Y)}) J_{X(Y)}.
\end{aligned} \tag{50}$$

According to the first law of thermodynamics, the energy flow $\dot{E}_{X(Y)}$ into the subsystem reads

$$\begin{aligned}
\dot{E}_{X(Y)} &= \dot{Q}_{X(Y)L} + \dot{Q}_{X(Y)R} + \dot{W}_{X(Y)} \\
&= -T\mathcal{F}_{X(Y)}\left(C_1^G\right) J\left(C_1^G\right),
\end{aligned} \tag{51}$$

depending on the Coulomb force and the global current. The steady-state internal energy of the bipartite system remains constant, $\left(d_t E = \dot{E}_X + \dot{E}_Y = 0\right)$. Multiplying Eq. (46) by T and applying the above derivatives, one obtains

$$T\dot{\sigma}_{X(Y)} = \dot{W}_{X(Y)} - \dot{F}_{X(Y)} \geq 0, \tag{52}$$

where the rate of partial nonequilibrium free energy $\dot{F}_{X(Y)}$ associated with X (Y) is defined as[29,31]

$$\dot{F}_{X(Y)} = \dot{E}_{X(Y)} + T\dot{I}_{X(Y)}. \tag{53}$$

Equation (52) provides an extension of the second law of thermodynamics, which offers an upper bound for the maximum work flux of the subsystem. The flow rate of partial nonequilibrium free energy can be partitioned into information-related and energy-related parts. Its definition has been generally found appropriately, because $\dot{I}_{X(Y)}$ is equivalent to the flow rate of the Shannon entropy of the system $\dot{S}$ due to the interaction with reservoirs XL (YL) and XR (YR).

3. Results and discussion

Without loss of generality, we control over the tunnel rate in the weak coupling regime. To reduce the number of parameters, the tunneling rates are parameterized by just two dimensionless parameters Δ and δ:

$$\begin{aligned}
\Gamma_{x_0}^{(XL)} &= \Gamma\frac{e^{+\delta}}{\cosh(\delta)}, \quad \Gamma_{x_1}^{(XL)} = \Gamma\frac{e^{-\delta}}{\cosh(\delta)}, \\
\Gamma_{x_0}^{(XR)} &= \Gamma\frac{e^{-\delta}}{\cosh(\delta)}, \quad \Gamma_{x_1}^{(XR)} = \Gamma\frac{e^{+\delta}}{\cosh(\delta)}, \\
\Gamma_{y_0}^{(YL)} &= \Gamma\frac{e^{+\Delta}}{\cosh(\Delta)}, \quad \Gamma_{y_1}^{(YL)} = \Gamma\frac{e^{-\Delta}}{\cosh(\Delta)}, \\
\Gamma_{y_0}^{(YR)} &= \Gamma\frac{e^{-\Delta}}{\cosh(\Delta)}, \quad \Gamma_{y_1}^{(YR)} = \Gamma\frac{e^{+\Delta}}{\cosh(\Delta)}.
\end{aligned}$$

In addition, we set $C_{XL} = C_{XR} = C_{YL} = C_{YR} = C_0$.

Figure 4(a) shows currents of fundamental cycles selected in Eq. (30). When dot Y (X) is empty, the local cycle current $J(C_1^X) < 0$ (black dot-dot-dashed line) [$J(C_1^Y) < 0$ (black dashed line)], meaning that electrons are prone to transfer from the higher chemical potential to the lower chemical potential. When Y is occupied, the local cycle current $J(C_2^X)$ (red dash-dotted line) through X does not move in a fixed direction, but is embodied in two situations. The first case is characterized by $J(C_2^X) > 0$ in the small-$\Delta\mu_X$ regime ($\Delta\mu_X < \Delta\mu_0$), where the Coulomb coupling and information exchange between X and Y allow electrons transfer from reservoir XL with lower chemical potential to reservoir XR with higher chemical potential. The second case is characterized by $J(C_2^X) < 0$ in the large-$\Delta\mu_X$ regime ($\Delta\mu_X > \Delta\mu_0$), because the thermodynamic force $-\mathcal{F}(C_2^X)$ dominates the electron transport again. When X is occupied, the local cycle current $J(C_2^Y)$ (red dashed line) changes from negative to positive as $\Delta\mu_X$ increases. When $\Delta\mu_X$ is large enough, the dot X may provide enough energy or

information for driving the electron flow in the direction opposite to the chemical potential gradient $-F(C_2^Y)$. The graph theory offers an effective way to unearthing the fundamental path, where the current through one dot could drag the current through the other dot.

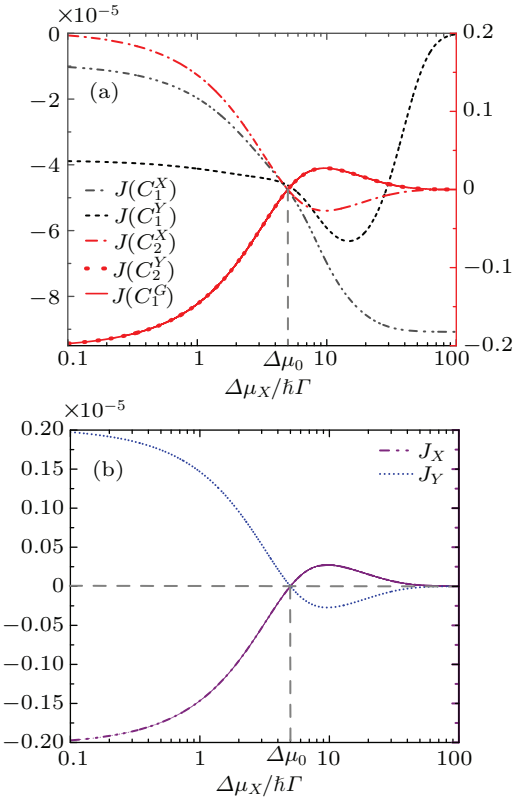


Fig. 4. The curves of (a) the cycle currents and (b) the electronic currents J_X and J_Y in units of $\hbar\Gamma$, varying with the chemical potential difference $\Delta\mu_X/\hbar\Gamma$. The left vertical axis shows values for $J(C_1^X)$ and $J(C_2^X)$, while the corresponding scales of $J(C_1^G)$, $J(C_1^Y)$, and $J(C_2^Y)$ are on the right vertical axis. The parameters $\varepsilon_X = 0$, $\varepsilon_Y = 0$, $\Delta\mu_Y = 5.0\hbar\Gamma$, $\mu_{XL} - \mu_{YL} = 1.0\hbar\Gamma$, $C = 0.5q^2/\hbar\Gamma$, $C_0 = 1.0q^2/\hbar\Gamma$, $k_BT = 1.0\hbar\Gamma$, and $\Delta = \delta = 5.0$. These values are used unless otherwise mentioned specifically in the following discussion.

In the regime of small $\Delta\mu_X$, the direction of the global cycle current is counterclockwise $J(C_1^G) < 0$. According to Eq. (51), multiplying $J(C_1^G)$ by the partial affinities $-\mathcal{F}_X\left(C_1^G\right)$ and $-\mathcal{F}_Y\left(C_1^G\right)$, respectively, we know that the energy flow is fed from X to Y (grey dot-dot-dashed lines Fig. 5). In the latter, the direction of the global cycle current becomes clockwise as $\Delta\mu_X$ increases, which lies the regime suitable for the energy flowing from Y to X. By applying Eqs. (31) and (32), Fig. 4(b) presents the net electronic currents from XR to XL (J_X) and from YR to YL (J_Y). Owing to the existence of electron–electron interaction, the local cycle current $J(C_2^X)$ $\left[J(C_2^Y)\right]$ makes a major contribution to the current J_X (J_Y). For $\Delta\mu_X < \Delta\mu_0$, the net electronic current J_X flows from reservoir XL with lower chemical potential to reservoir XR with higher chemical potential. The work flux $\dot{W}_X < 0$ (black solid line in Fig. 5), so that dot X produces power output. As $\Delta\mu_X$ gets larger, the situation is exactly the opposite. The net electronic current J_Y flows against the bias due to the thermodynamic force and dot Y starts to generate positive power output.

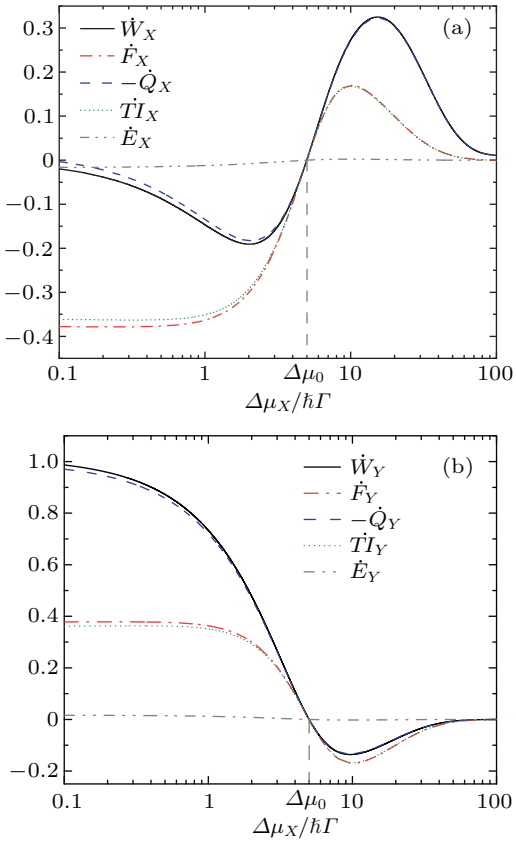


Fig. 5. The work fluxes (black solid lines), rates of partial nonequilibrium free energy (red dash-dotted lines), heat currents (blue dashed lines), information flows (green dotted lines), and energy flows (grey dot-dot-dashed lines) of the subsystems (a) X and (b) Y, in units of $\hbar\Gamma$, varying with the chemical potential difference $\Delta\mu_X/\hbar\Gamma$ at steady state.

The currents of fundamental cycles are more important to investigate the thermodynamics of the rates of partial nonequilibrium free energy (red dash-dotted lines) and information flows (green dotted lines). The nonequilibrium Clausius and free energy inequalities [Eqs. (46) and (52)] serve the subsystems with the local second law of thermodynamics, which are demonstrated in Fig. 5. They behave equivalently and complement each other for a unify treatment of temperature. For $\Delta\mu_X < \Delta\mu_0$, the total heat current into X, $\dot{Q}_X = \dot{Q}_{XR} + \dot{Q}_{XL} > 0$. To achieve this effect, a noticeable information flowing from Y to X guarantees that $T\dot{\sigma}_X = -\dot{Q}_X - T\dot{I}_X > 0$. The information flow benefits from the current of the global cycle $J\left(C_1^G\right)$ driven by the information affinity $\mathcal{F}_I\left(C_1^G\right)$. At the same time, dot X performs work $\dot{W}_X < 0$, which is enabled by the negative rate of partial nonequilibrium free energy $0 > \dot{W}_X > \dot{F}_X$. Note that these effects are compensated by the dissipation of work into heat in dot Y. For $\Delta\mu_X$¿$\Delta\mu_0$, the roles of X and Y are totally reversed. It should be emphasized that under most conditions the power output is generated due to the feedback-induced information flow and not due to energy flow, because $\dot{E}_{X(Y)} \approx 0$ and $\dot{F}_{X(Y)} \approx T\dot{I}_{X(Y)}$. As a result, the nonequilibrium double quantum-dot system works as

a quantum autonomous Maxwell demon at the cost of information without violating the second law of thermodynamics.

4. Conclusion

In summary, the present work reveals the local second law of thermodynamics of Coulomb-coupled double quantum dots. The graph theory has proved that the entropy production and nonequilibrium free energy are closely related to information flow and affinities. The information flow between the subsystems acts as a driving force for the global cycle to pump electrons against the bias voltage. The proposed model offers possible schemes to design nanoelectronic devices through the control of cycle fluxes.

References

[1] Callen H B 1985 *Thermodynamics and an Introduction to Thermostatistics* (New York: John Wiley & Sons)
[2] Gao T F, Zhang Y and Chen J C 2009 *Chin. Phys* **18** 3279
[3] Onsager L 1931 *Phys. Rev. B* **37** 405
[4] Gaspard P 2013 *New J. Phys.* **15** 115014
[5] Benenti G, Casati G, Saito K and Whitney R S 2017 *Phys. Rep.* **694** 1
[6] Ren J 2017 *Front. Phys.* **12** 120505
[7] Andrieux D and Gaspard P 2008 *Proc. Natl. Acad. USA* **105** 9516
[8] Schnakenberg J 1976 *Rev. Mod. Phys.* **48** 571
[9] Horowitz J M and Esposito M 2014 *Phys. Rev. X* **4** 031015
[10] Yamamoto S, Ito S, Shiraishi N and Sagawa T 2016 *Phys. Rev. E* **94** 052121
[11] Seifert U 2012 *Rep. Prog. Phys.* **75** 126001
[12] Einax M and Nitzan A 2016 *J. Chem. Phys.* **145** 014108
[13] Andrieux D and Gaspard P 2007 *J. Stat. Phys.* **127** 107
[14] Taniguchi N 2018 *Phys. Rev. B* **97** 155404
[15] Anders J and Esposito M 2017 *New J. Phys.* **19** 010201
[16] Peusner L 1986 *Studies in Network Thermodynamics* (Amsterdam: Elsevier)
[17] Peusner L 1982 *J. Chem. Phys.* **77** 5500
[18] Peusner L 1985 *J. Chem. Phys.* **83** 1276
[19] Peusner L, Mikulecky D C, Bunow B and Caplan S R 1985 *J. Chem. Phys.* **83** 5559
[20] Peusner L 1983 *J. Theor. Biol.* **102** 7
[21] Peusner L 1985 *J. Theor. Biol.* **115** 319
[22] Peusner L 1970 *The Principles of Network Thermodynamics and Biophysical Applications* PhD Dessertation (Harvard University) (reprinted by Entropy: Lincoln, MA, 1987)
[23] Crooks G E 1998 *J. Stat. Phys.* **90** 1481
[24] Crooks G E 1999 *Phys. Rev. E* **60** 2721
[25] Esposito M, Harbola U and Mukamel S 2009 *Rev. Mod. Phys.* **81** 1665
[26] Vaikuntanathan S and Jarzynski C 2008 *Phys. Rev. Lett.* **100** 190601
[27] Jarzynski C 1997 *Phys. Rev. Lett.* **78** 2690
[28] Huber G, Schmidt-Kaler F, Deffner and Lutz S E 2008 *Phys. Rev. Lett.* **101** 070403
[29] Esposito M and Van den Broeck C 2011 *Europhys. Lett.* **95** 40004
[30] Esposito M, Lindenberg K and Van den Broeck C 2010 *New J. Phys.* **12** 013013
[31] Ptaszyński K and Esposito M 2019 *Phys. Rev. Lett.* **122** 150603
[32] Deffner S and Jarzynski C 2013 *Phys. Rev. X* **3** 041003
[33] Lin Z, Shen W, Su S and Chen J 2020 *Acta Phys. Sin.* **69** 130501 (in Chinese)
[34] Miyahara H and Aihara K 2018 *Phys. Rev. E* **98** 042138
[35] Sagawa T and Ueda M 2010 *Phys. Rev. Lett.* **104** 090602
[36] Barato A C and Seifert U 2014 *Phys. Rev. Lett.* **112** 090601
[37] Peng P and Duan C 2016 *Chin. Phys. Lett.* **33** 080501
[38] Cao L, Ke P, Qiao L Y and Zheng Z G 2014 *Chin. Phys.* **23** 070501
[39] Horowitz J M 2015 *J. Stat. Mech. Theor. Exp.* **2015** P03006
[40] Chapman A and Miyake A 2015 *Phys. Rev. E* **92** 062125
[41] Soltanmanesh A and Shafiee A 2019 *Eur. Phys. J. Plus* **134** 282
[42] Marconi U M B, Puglisi A and Maggi C 2017 *Sci. Rep.* **7** 46496
[43] Bertini L, De Sole A, Gabrielli D, Jona-Lasinio G and Landim C 2015 *J. Stat. Mech. Theor. Exp.* **2015** P10018
[44] Zhang Y, Huang C, Wang J, Lin G and Chen J 2015 *Energy* **85** 200
[45] Sánchez R and Bütiker M 2011 *Phys. Rev. B* **83** 085428
[46] Chen X and Wang C 2019 *Chin. Phys. B* **28** 050502
[47] Wang C and Xu D 2020 *Chin. Phys. B* **29** 080504
[48] Lu X, Zhang J and Xia Y 2021 *Chin. Phys. B* **30** 020301
[49] Orszag M 2016 *Quantum Optics: Including Noise Reduction, Trapped Ions, Quantum Trajectories, and Decoherence* (New York: Springer)
[50] Rodrigo R S 2007 *Spin and Charge Transport through Driven Quantum Dot Systems and Their Fluctuations* (PhD Dessertation, Universidad Autónoma de Madrid)
[51] Sothmann B, Sánchez R and Jordan A N 2015 *Nanotechology* **26** 032001
[52] Spohn H 1978 *J. Math. Phys.* **19** 1227
[53] Esposito M, Harbola U and Mukamel S 2007 *Phys. Rev. E* **76** 031132
[54] Schaller G 2014 *Open Quantum Systems Far from Equilibrium* (New York: Springer)
[55] Shi Z, Fu J, Qin W and He J 2017 *Chin. Phys. Lett.* **34** 110501
[56] Shiraishi N and Sagawa T 2015 *Phys. Rev. E* **91** 012130